Dark-Current Random Telegraph Signal in InGaAs Image Sensor for SWIR domain

M. Benfante, C. Durnez, V. Lalucaa, A. Rouvie, A. Le Roch and C. Virmontois

***Abstract*— The Dark Current Random Telegraph Signal is observed and investigated in small pitch InGaAs-based SWIR image sensors. This phenomenon corresponds to dark signal fluctuation and is related to blinking pixels. It is a major issue in image sensors because of the random behavior which is impossible to calibrate. In this work, the readout noise, the dark current and the DC-RTS are studied in two commercial of the shelf InGaAs image sensor formats.**

***Index Terms*— Infrared, SWIR, InGaAs image sensor, Dark Current Random Telegraph Signal, noise, blinking pixel.**

I. Introduction

SHORT Wavelength InfraRed (SWIR) imaging is currently undergoing rapid interest for commercial and space applications, including optical telecommunication, remote monitoring and scientific imaging such as atmosphere sounding, Earth observation and planetology to study the mineral composition of celestial body's regolith. Indium-Gallium-Arsenide (InGaAs) image sensors operating close to ambient temperature in the spectral range of 0.8 to 1.7 µm are ideal candidates to meet missions' requirements. CNES (French Space Agency) is working on several InGaAs image sensors over the last decades [1]-[4] to increase the Technical Readiness Level (TRL) of such technology in space. While these sensors present very interesting electro-optical performances in SWIR domain, a particular attention is made on noises, dark current and dark current fluctuation also known as Random Telegraph Signal (RTS). This latter phenomenon can be described as blinking pixel in the dark (without illumination). This parasitic signal variation is a major issue for scientific imaging instrument as it cannot be calibrated. Moreover, the large signal amplitudes observed lead to corrupted pixel value. This phenomenon is well kwon is silicon-based image sensor [5]-[7] but rarely reported in InGaAs sensor literature [8] or other Infrared sensors as Mercury Cadmium Telluride [9].

In this study, DC-RTS is investigated in 5µm (IMX990/991) and 3.45µm (IMX992) pixel pitches, using direct Cu-Cu bonding InGaAs image sensors [10]. All the presented results are pristine in engineering samples. First, the activity focuses on readout noise. This noise background will serve as the RTS pixel detection threshold. Then, dark current and activation energy are discussed before focusing on DC-RTS. The number of RTS pixels, the number of RTS levels, the mapping and the RTS amplitude distribution are reported and discussed.

M. Benfante is with Expleo France, Toulouse, 31300, France.
C. Durnez, V. Lalucaa, A. Rouvié, A. Le Roch and C. Virmontois are with the Centre National d'Etudes Spatiales (CNES), Toulouse, 31000, France (e-mail: cedric.virmontois@cnes.fr).

II. Experimental Details

The characterization of the IMX SWIR sensors has been performed at different temperatures (between 10 to 50°C), integration times (from few milliseconds to several seconds), exposure modes and gains. Two exposure and reading modes are possible for the IMX992: The Global Shutter (GS) and the Dual Read Rolling Shutter (DRRS). The conversion gain is distinguished in the High Conversion Gain (HCG) and Low Conversion Gain (LCG).

- Noise: The noise has been evaluated in GS-LCG, GS-HCG and DRRS-HCG
- *Dark Current*: The dark current has been measured in both GS and DRRS modes and tested with LCG and High Conversion Gain HCG.
- *Dark Current Random Telegraph Signal*: The DC-RTS has been measured in *GS-LCG* mode.

Regarding the IMX990/991, only one gain and GS exposure mode has been employed. The dark current has been measured between 11°C and 44°C for the IMX990/991 and for the IMX992. DC-RTS has been studied at the same temperatures for IMX992 and at 15°C and 39°C for the IMX990/991.

III. Noise, CVF and Full Well

The noise has been computed as the standard deviation of the temporal fluctuation of the output signal. At minimal integration time, the noise corresponds to the read-out noise. Table I and Table II show read-out noise for the IMX992 and IMX990/991 respectively. It has been computed as an average over all the pixels. Fig.1 shows the noise as a function of the integration time and the read-out noise for the IMX992 29 °C in GS-LCG mode. CVF and Full Well have been extracted in each mode using the Photon Transfer Curve method.

TABLE I
IMX992 MEASURED PARAMETERS AT 29 °C AT DIFFERENT EXPOSITION METHODS AND GAINS

	GS LCG	GS HCG	DRRS HCG
Read-Out Noise (e^-_{rms})	187	107	29
CVF (DN/e^-)	0.059	0.101	0.106
Full Well (e^-)	68 600	40 500	38 600

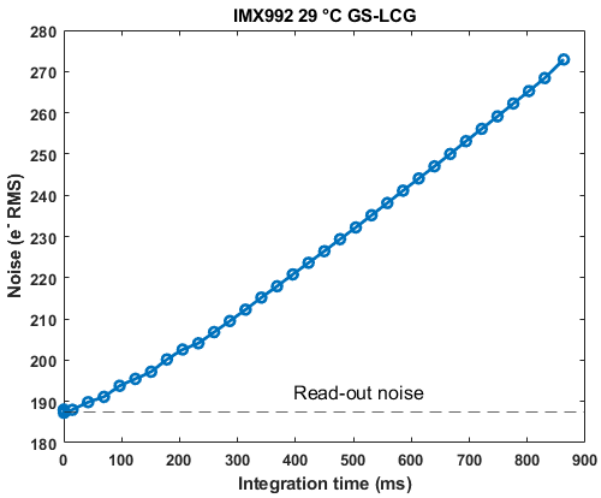

Fig. 1. Noise as a function of integration time at 29 °C for IMX992 in GS LCG.

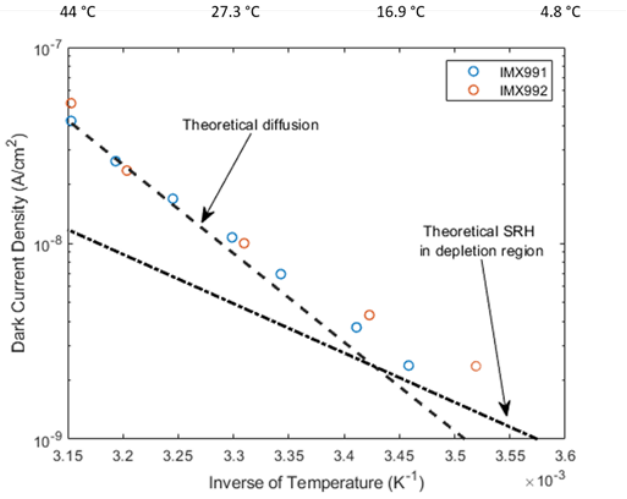

Fig. 2. Arrhenius plot of average dark current density. A comparison between IMX991 and IMX992

TABLE II
IMX990/IMX991 MEASURED PARAMETERS AT 29°C

	GS
Read-Out Noise (e^-_{rms})	190
CVF (DN/e^-)	0.023
Full Well (e^-)	178 000

IV. DARK CURRENT

For each temperature, the dark current is extracted for every pixel as the slope of the linear fit between the dark signal and the integration time and converted to electron or ampere using the conversion gain extracted through the Photon Transfer Curve method.

Fig. 2 shows the average dark current density at each measured temperature for IMX991 and 992. Theoretical dark current from diffusion process or SHR process have been added in dash line to be compare to data. The results spread between the diffusion limit (activation energy of 0.9 eV corresponding to InGaAs gap) at high temperature and the SRH generation in depletion region limit (activation energy of 0.5 eV corresponding to InGaAs mid-gap). Interestingly, the IMX991 and IMX992 have comparable dark current density at high temperature. This observation indicates that bulk diffusion current dominates at high temperature [11] whatever the pixel pitch. This means that diffusion contribution should be the same whatever the pixel surface. At lower temperature IMX992 shows higher dark current density indicating that defect-induced SRH generation in depletion region should not be related to surface mechanism but probably to the thickness or perimeter. The greater relative importance of SRH mechanisms can be ascribed to higher relative depletion region volume with respect to non-depleted volume and also to higher influence of the InGaAs/InP depleted interface.

Fig. 3 shows dark current histogram and it associated per-pixel activation energy. The highest dark current pixels are dominated by SRH in depletion region (activation energy of 0.5 eV). This result could confirm that Electric Field Enhancement (EFE) is not acting in this device.

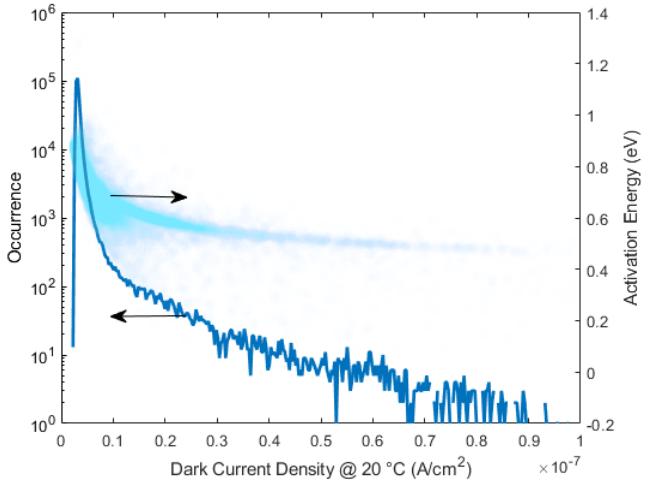

Fig. 3. Relation between dark current density and it activation energy.

V. DARK CURRENT RANDOM TELEGRAPH SIGNAL

The DC-RTS has been analyzed using a specific algorithm [12] based on a classical edge detection technique. The time between two successive acquisitions was of 2s both for IMX990/991 and IMX992. All RTS measurement conditions are summarized in Table III.

TABLE III
PARAMETER USED TO ANALYZED THE DC-RTS

Parameter	Value
Time between two images	2 s
Number of images	2500
Number of analyzed pixels	500 x 500
Number of filter coefficients	18

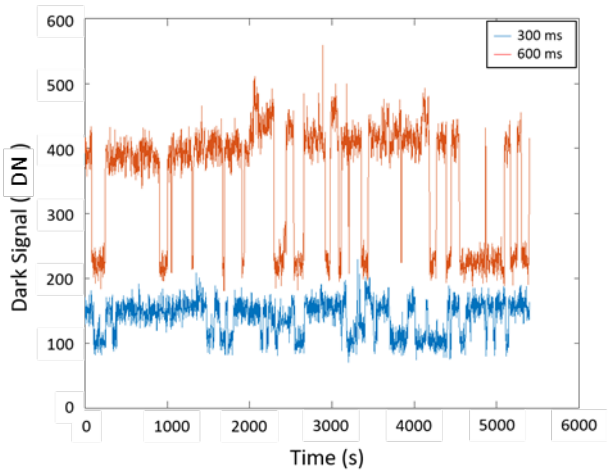

Fig. 4. Example of DC-RTS track at two integration times at 29 °C in IMX992.

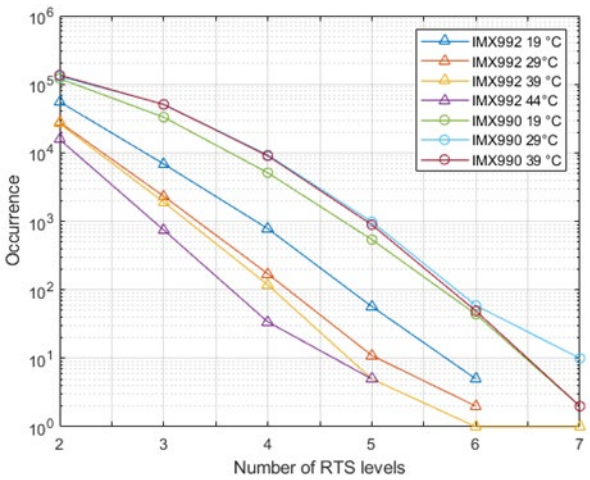

Fig. 6. Histogram of RTS pixels according to the number of RTS levels.

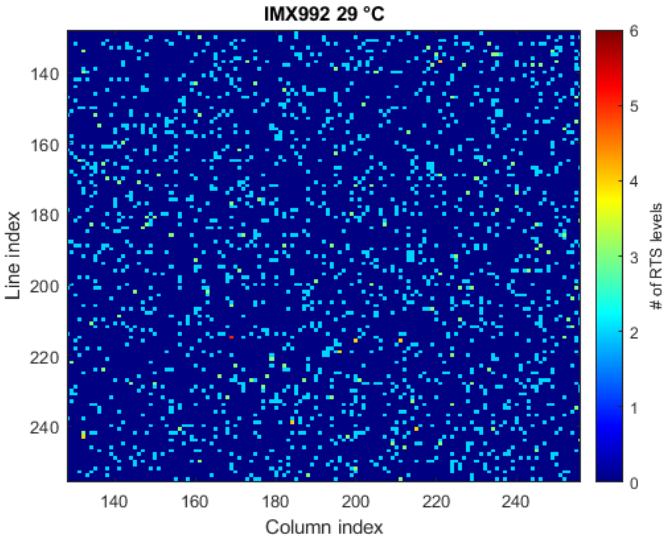

Fig. 5. Cartography of RTS pixels and number of RTS levels in an area. The total number of analyzed pixels was 500 x 500 = 250 000

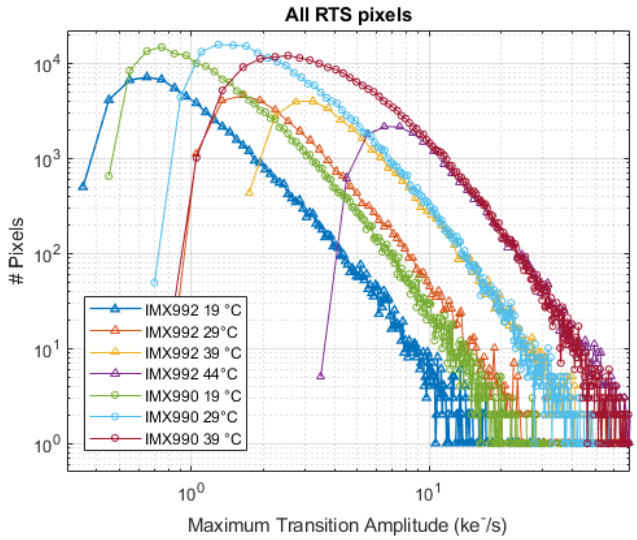

Fig. 7. Maximum transition amplitude as function of temperature for IMX990 and IMX992 in log-log scale.

Fig. 4 shows an example of DC-RTS track at two integration times. Increasing the integration time increases the transition amplitudes confirming the origin of DC-RTS from the photodiode. Indeed, RTS signals coming from ROIC transistors are independent on integration time.

Fig. 5 shows RTS pixels mapping for a centered 500x500-pixel area in IMX992. The RTS pixels are uniformly distributed over the array. The color of the RTS pixel corresponds to the number of RTS levels. 2-level RTS pixels constitute the main population of RTS pixels. As observed in Fig. 6 on the RTS pixel histogram, the number of RTS level are exponentially distributed from 2 to a maximum of 7 levels. The number of detected RTS pixels depend of the noise at measured temperature and the observation time. This can explain the change of the detected RTS numbers.

Fig. 7 shows the maximum transition amplitude (MTA) distribution for both pixel pitches at different temperatures. The exponential behavior previously observed in silicon-based and other semiconductor-based sensor [3]-[4], [9], [12], [13] are confirmed in the investigated technology. It is clearly observed that amplitudes increase with temperature. At the same temperature the results should be the same whatever the pixel pitch but a little discrepancy is observed. This could be due to temperature variation from one sensor to the other, as the power consumption is different. Further analyzes are need to better understand the physical insights.

Fig. 8 focuses on one distribution in log-linear scale. The data have been fitted through an exponential model [12]. As can be seen, the distribution presents two trends. Using the exponential law, the two average values have been extracted. The MTA ranges from 540 e/s to 1900 e/s at 19°C. Results could be explained either by two populations of RTS pixels with different lambda, or most likely, a single RTS mechanism impacted by local electric field enhancement EFE that tend to bend the distribution toward higher MTA. However, as dark current activation energy does not lead to EFE, it will be interesting to evaluate MTA activation energy to clarify this results.

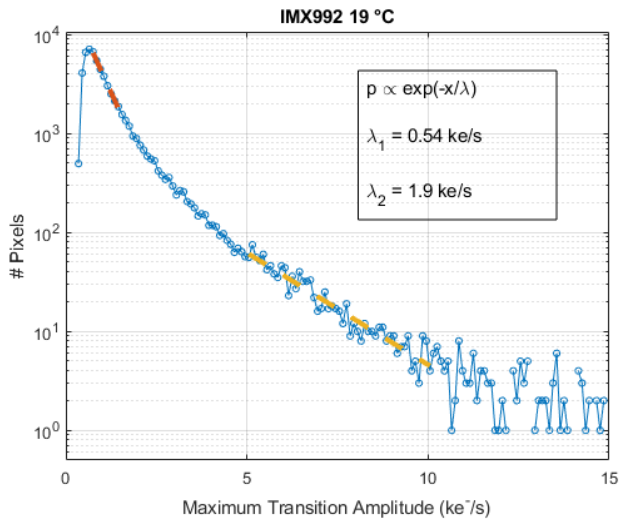

Fig. 8. Maximum transition amplitude histogram for IMX992 at 20 °C in log-linear scale. The exponential model fit is added.

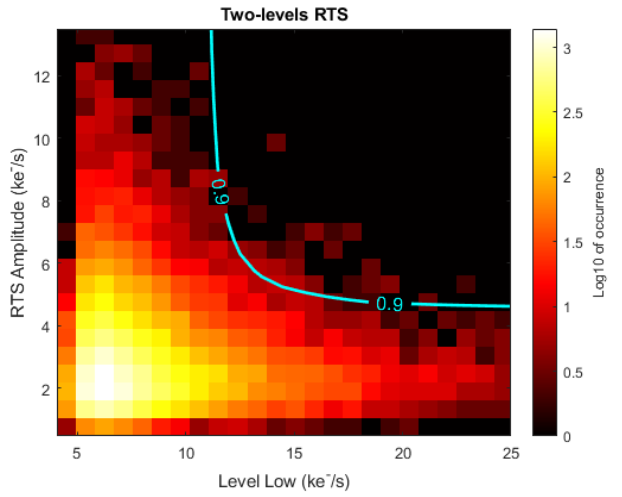

Fig. 9. Maximum transition amplitude as function of low level dark current. Results show highest amplitude in case of smallest low level.

A general trend that has been found during 2-levels DC-RTS analysis, as shown in Fig. 9 is that the higher transition amplitudes occur for the smaller low level of the DC-RTS.

VI. Conclusion

This paper presents one of the first study focused on DC-RTS in InGaAs SWIR image sensor. Two devices have been tested with different pixel pitches. First, noises and dark current are deeply analyzed, then, RTS pixels, also referred blinking pixels, have been reported in both pristine devices. The number of RTS pixel, the number of RTS level and the Maximum Transition Amplitude have been calculated and investigated to provide new insight of this random phenomenon. As previously reported in silicon-based devices, the RTS amplitude increase with integration time meaning that the photodiode is involve. The uniform mapping of detected RTS pixel, the number of RTS level found and the exponential distribution of the MTA are also in good agreement with the silicon literature. DC-RTS seems to be a common phenomenon in several semiconductor materials used to process image sensors. The large RTS amplitudes reported increase with temperature. These values reach hundreds of ke⁻/s that could reduce an important percentage of the pixel dynamic for long integration time around the second. Further works on these devices and InGaAs sensors are needed to properly understand DC-RTS behavior origins. DC-RTS is mainly attributed to meta-stable center in the semiconductor bulk that present a variation of the generation rate. As in silicon, these meta-stable centers are probably intrinsic defects in the crystal lattice located in the photodiode depleted area.

References

[1] D. Herve et al. “SPOT 4’s HRVIR and Vegetation SWIR cameras,” Proc. SPIE 2552, Infrared Technology XXI, (8 September 1995); https://doi.org/10.1117/12.218284.

[2] O. Gilard et al., "Damage Factor for Radiation-Induced Dark Current in InGaAs Photodiodes," in IEEE Transactions on Nuclear Science, vol. 65, no. 3, pp. 884-895, March 2018, doi: 10.1109/TNS.2018.2799742.

[3] V. Lalucaa, L. Calvinhac and C. Virmontois, "Dark Current Random Telegraph Signal in visible and SWIR Direct Cu-Cu bonding InGaAs Image Sensor," 2021 21th European Conference on Radiation and Its Effects on Components and Systems (RADECS), Vienna, Austria, 2021, pp. 1-4.

[4] C. Virmontois et al., "Dark Current Random Telegraph Signals in Short-Wavelength Infrared Image Sensors Based on InGaAs," in IEEE Transactions on Nuclear Science, vol. 68, no. 5, pp. 770-776, May 2021, doi: 10.1109/TNS.2021.3074052.

[5] I. H. Hopkins and G. R. Hopkinson, “Random telegraph signals from proton-irradiated CCDs,” *IEEE Trans. Nucl. Sci.*, vol. 40, no. 6, pp. 1567–1574, Dec. 1993.

[6] I. H. Hopkins and G. R. Hopkinson, “Further measurements of random telegraph signals in proton irradiated CCDs,” *IEEE Trans. Nucl. Sci.*, vol. 42, no. 6, pp. 2074–2081, Dec. 1995.

[7] G. R. Hopkinson, “Radiation effects in a CMOS active pixel sensor,” IEEE Trans. Nucl. Sci., vol. 47, no. 6, pp. 2480–2484, Dec. 2000.

[8] G. R. Hopkinson, R. H. Sorenson, B. Leone, R. Meynart, A. Mohammadzadeh and W. Rabaud, “Radiation effects in InGaAs and microbolometer infrared sensor arrays for space applications,” *IEEE Trans. Nucl. Sci*., vol. 55, no. 6, pp. 3483–3493, Dec. 2008.

[9] C. Virmontois, V. Goiffon, M. S. Robbins, L. Tauzième, H. Geoffray, M. Raine, S. Girard, O. Gilard, P. Magnan, and A. Bardoux, “Dark current random telegraph signals in solid-state image sensors,” *IEEE Trans. Nucl. Sci.*, vol. 60, no. 6, pp. 4323–4331, Dec. 2013.

[10] S. Manda, R. Matsumoto, S. Saito, S. Maruyama, H. Minari, T. Hirano, T. Takachi, N. Fujii, Y. Yamamoto, Y. Zaizen, et al., “High-definition Visible-SWIR InGaAs Image Sensor using Cu-Cu Bonding of III-V to Silicon Wafer.,” *in 2019 IEEE International Electron Devices Meeting (IEDM)*, pp. 16.7.1–16.7.4, Dec. 2019.

[11] M. Benfante, “Radiation effects on InGaAs infrared detectors,” PhD thesis 2024.

[12] V. Goiffon, G. R. Hopkinson, P. Magnan, F. Bernard, G. Rolland and O. Saint-Pe, "Multilevel RTS in Proton Irradiated CMOS Image Sensors Manufactured in a Deep Submicron Technology," *IEEE Trans. on Nucl. Sci.*, vol. 56, no. 4, pp. 2132-2141, Aug. 2009.

[13] C. Durnez, V. Goiffon, C. Virmontois, P. Magnan and L. Rubaldo, "Comparison of Dark Current Random Telegraph Signals in Silicon and InSb-Based Photodetector Pixel Arrays," *IEEE Trans. Elect. Dev.*, vol. 67, no. 11, pp. 4940-4946, Nov. 2020.